AIP | Journal of Applied Physics

Painting cracks: A way to investigate the pictorial matter

Frédérique Giorgiutti-Dauphiné and Ludovic Pauchard

Citation: Journal of Applied Physics **120**, 065107 (2016); doi: 10.1063/1.4960438
View online: http://dx.doi.org/10.1063/1.4960438
View Table of Contents: http://scitation.aip.org/content/aip/journal/jap/120/6?ver=pdfcov
Published by the AIP Publishing

JOURNAL OF APPLIED PHYSICS **120**, 065107 (2016)

Painting cracks: A way to investigate the pictorial matter

Frédérique Giorgiutti-Dauphiné and Ludovic Pauchard
Laboratoire FAST, Univ. Paris-Sud, CNRS, Université Paris-Saclay, F-91405 Orsay, France

(Received 14 June 2016; accepted 23 July 2016; published online 11 August 2016)

An old painting generally exhibits a wide variety of crack patterns. From a strictly aesthetic point of view, cracks are undesirable; nevertheless, they can be seen as the fingerprints of the painting and provide valuable knowledge about the art piece. Precisely, the morphology of crack patterns can be related to the mechanical properties of the pictorial matter or they can reveal information about the methods used by the artist or the conditions of conservation. In the present paper, we show how drying dispersions of colloidal particles in a volatile solvent on a non-porous substrate provides a good candidate to study crack formation in a solid layer. We recover the crack patterns observed in paintings, and we investigate the role of the substrate, e.g., the sub-layer, and of the thickness of the layer in the crack spacing. We show how to deduce mechanical properties of a sub-layer, provided the thickness and the elastic modulus of the layer are known. These experiments aim to propose a potentially non-invasive method to deduce quantitative information about mechanical properties of a pictorial matter which could be of great interest for cultural heritage. *Published by AIP Publishing.* [http://dx.doi.org/10.1063/1.4960438]

I. INTRODUCTION

A painting is a complex system, both from a geometrical and a physicochemical point of views. The pictorial layer is a multi-layer structure on a deformable support (canvas or panel). This multilayer system consists of ground, different layers of paint, and finally a varnish layer for old paintings. The composition of the paint is also complex, and its formulation is not a standard feature as it can vary a lot from one product to another. Nevertheless, the main components are solid pigments (metal oxides or metal salts) and binding medium. The oldest binding medium is egg tempera (mixture of egg yolk as binding agent with colored pigments), used until the end of the 15th century. Then, artists used drying oil until the beginning of the 20th century, when acrylic paint was started being used with the binder being an aqueous acrylic polymer emulsion. Different kinds of additives can be mixed in the paint to change its viscosity, its mechanical properties, or its stability such as surfactant, plasticizer, or solvent. The drying oil is made of triglycerides which can be polyunsaturated or monounsaturated. The most common drying oils encountered are linseed, poppy, and safflower oil. The drying consists of a chemical drying where successive oxidative and polymerization processes lead to the formation of a tridimensional network and of a solid film where the pigment particles are entangled and bound. Finally, the chemical composition of the successive layers in a painting is different, and each layer has distinctive boundary conditions (the layers are restrained by each other). This results in each layer exhibiting specific mechanical properties that contributes in their own way to the development of stresses in the pictorial layer. There are a number of sources for the development of stresses in a painting.[1] The first source is the tensile stress resulting from the drying process or from the chemical drying (cross-linking process). Additional stresses arise from environmental changes such as temperature or hygrometry variations. The support could undergo some stresses and deformations too. These deformations could be caused by environmental factors or due to some restoration processes such as restretching or lining. The consequences of these stresses in the pictorial layer are mechanical damages such as the formation of crack patterns which are the more undesirable aspect of aging. However, they can be of great interest in art paintings since the morphologies of crack patterns can reveal some properties of the pictorial matter or some information about the methods used by the artists which in turn can provide important details to authenticate paintings (fingerprints).[2] The diversity in materials and the complexity of the multi-layer system which forms the pictorial layer imply that the crack patterns are very diversified. Therefore, it seems to be a tricky task to give an exhaustive description of the different crack patterns. A relevant description should take into account the effect of physical or environmental factors. Many kinds of classifications have been proposed to categorize cracks by considering specific features of the crack pattern or by considering the type of craquelure.[3,4] There are two main types of craquelure: the drying cracks (or premature cracks) and the age cracks. The first ones are induced by the drying process (physical or chemical drying) and occur in the first days of a painting in a ductile material. The penetration of these cracks is limited to a maximum of two layers in the painting. The second type of craquelure occurs later in the life of the paint film (maybe after many decades) and results from brittle fracture. After some time, the pictorial layer becomes brittle and cannot withstand the stress due to environmental changes. Compared to the drying cracks, these cracks have sharp edges, they penetrate deeper in the layers, and their width is smaller than the premature cracks. These cracks come from impact, deformation of the support, environmental changes, or changes in the structure due to aging processes such as oxidation. A network of fine cracks is usually associated with aging cracks. Among the different works,[3,5,6] we refer to Stout's work[4] which has

proposed a complete classification taking into account both the type of cracks and the type of patterns, but the number of features to consider was too big and needed to be improved. A fuller and simplified description has been proposed by Bucklow in 1997.[3] He based his classification on the different paint traditions through centuries and countries, namely, French, Flemish, Dutch, and Italian. Thus, from these observations, he extracted seven features to distinguish between the following kinds of crack patterns: the direction of cracks (isotropic or anisotropic pattern), the shape of cracks (straight or curved), the connections between cracks, the distance between cracks, the thickness of the cracks, and the relationship between cracks' directions and the organization of cracks. We propose here to focus on four types of patterns which are among the most common, with "meaningful features."

II. CRACK PATTERNS IN PAINTINGS

Two types are observed in the multispectral image of the famous painting by Leonard da Vinci, *Mona Lisa*, in Figure 1-1 and result from different causes. The sky or the landscape reveals isotropic crack patterns due to the differential expansion of the pictorial layer arising with ageing; shrinkage is frustrated by adhesion on the sublayer. The same morphology can be obtained in drying cracks during the liquid-solid transition that is caused by evaporation from a dispersion of solid particles in a volatile solvent (Figure 1-1a) on a nonporous substrate. In these types of patterns, the cracks form through successive generations and divide the layer into polygonal fragments. A second type of pattern is observed in the carnation of the painting and consists in an array of parallel cracks lying along the direction of the grounds of the panel.

These cracks are deep and can propagate to the substrate. They can easily be associated with the deformation of the poplar panel with the variations of the surrounding humidity rate and temperature. This process can be reproduced with dispersion of solid particles, by stretching mainly in one direction, a brittle layer supported by a soft one. This results in a regularly spaced crack pattern in the brittle layer (Figure 1-1b). More generally, the crack spacing depends on the elastic modulus mismatch between the layer and the sublayer, and on the layer thickness. Therefore, significant deformation of the support possibly affects preferentially some regions of the pictorial layer (the face of *Mona Lisa*) rather than others (the landscape). This example shows that regions of the pictorial layer can easily release the deformation of the support, and exhibit crack pattern from other causes, whereas some regions directly transfer the deformation from the support. Consequently, we suggest that the material in the carnation is stiffer than the material used in the landscape. Some regions of the pictorial layer are free of cracks, like in the veil of *Mona Lisa*; here, Leonardo da Vinci applied his famous technique of Sfumato which consists in a layer-by-layer deposition of very thin layers of painting. Yet, below a critical thickness, films are usually crack-free, as the elastic energy stored in the material is not enough to produce cracks, as shown in experimental models (Figure 1-1c).[7–9]

Another type of pattern is observed in *La belle Ferronnière*, attributed to Leonard da Vinci, where the crack network shows no specific connections in a part of the face: this pattern is colored in red in the painting (Figure 1-2). This pattern is made of numerous crack junctions which form linear or star-like shapes that are initiated from nucleation centers in the layer. The density of junctions is high, but once nucleated, crack extent stops shortly before connection with adjacent junctions. This type of pattern attests that the nucleation of crack from defects is easier than their propagation through the layer. In particular, this example shows that the material is very sensitive to heterogeneities and the thickness of the layer should be of the same order of the heterogeneity size.[10]

Another criterion which can be taken into account is the width of the cracks; thus, large crack opening is visible in some pictorial layers. An example is presented in Figure 1-3 in *Jeanne d'Arc en prison* of Louis Crignier. Such a pattern attests to a strong shrinkage of a layer and a low adhesion on the sublayer. A similar morphology is observed in experimental models (image at right in Figure 1-3): a drying layer can shrink while it weakly adheres on the sublayer. This can be observed where a too much fatty oil is used for the sublayer that makes it very smooth. As a consequence, the paint layer does not adhere well to sublayer and can slide to produce large open cracks. Typical drying cracks appear few hours or days after painting.

From the above examples, it can be seen that the great variety of crack morphologies encountered in paintings appear to be specifically related to the material and the way the cracks are generated. As evidence, patterns of aging cracks as well as drying cracks can be recovered using model systems with tunable mechanical properties.

III. CRACK PATTERNS IN MODEL SYSTEMS

A. Systems

Model systems consist of aqueous colloidal dispersions of two equal-sized polystyrene nanoparticles, 30 nm in diameter (provided by Rhodia Recherche-Aubervilliers, France): stiff and soft particles. At room temperature, the stiff and soft particles exhibit a glass transition temperature of 100 °C and 16 °C, respectively. Glass transition temperatures T_g were estimated from the particle core composition. The initial volume fraction of both dispersions is 0.3. These dispersions are stable in the absence of evaporation. For each dispersion, the weak polydispersity of the particles size prevents crystallization (polydispersity, $\sim$0.18). Experiments were performed using either pure dispersions or binary mixtures of both dispersions. Binary mixtures are magnetically stirred and then sonicated. In a given layer, the volume fraction in deformable particles is denoted as ϕ. A layer is formed by depositing a controlled volume of a dispersion in a shallow and circular container (diameter, $\sim$30 mm and height, $\sim$5 mm). Then, the layer is left to dry from the free surface: the transfer of water in air is limited by diffusion and therefore controlled by the relative humidity $RH = 60\%$, at 20 °C. The solvent loss concentrates the dispersion, and

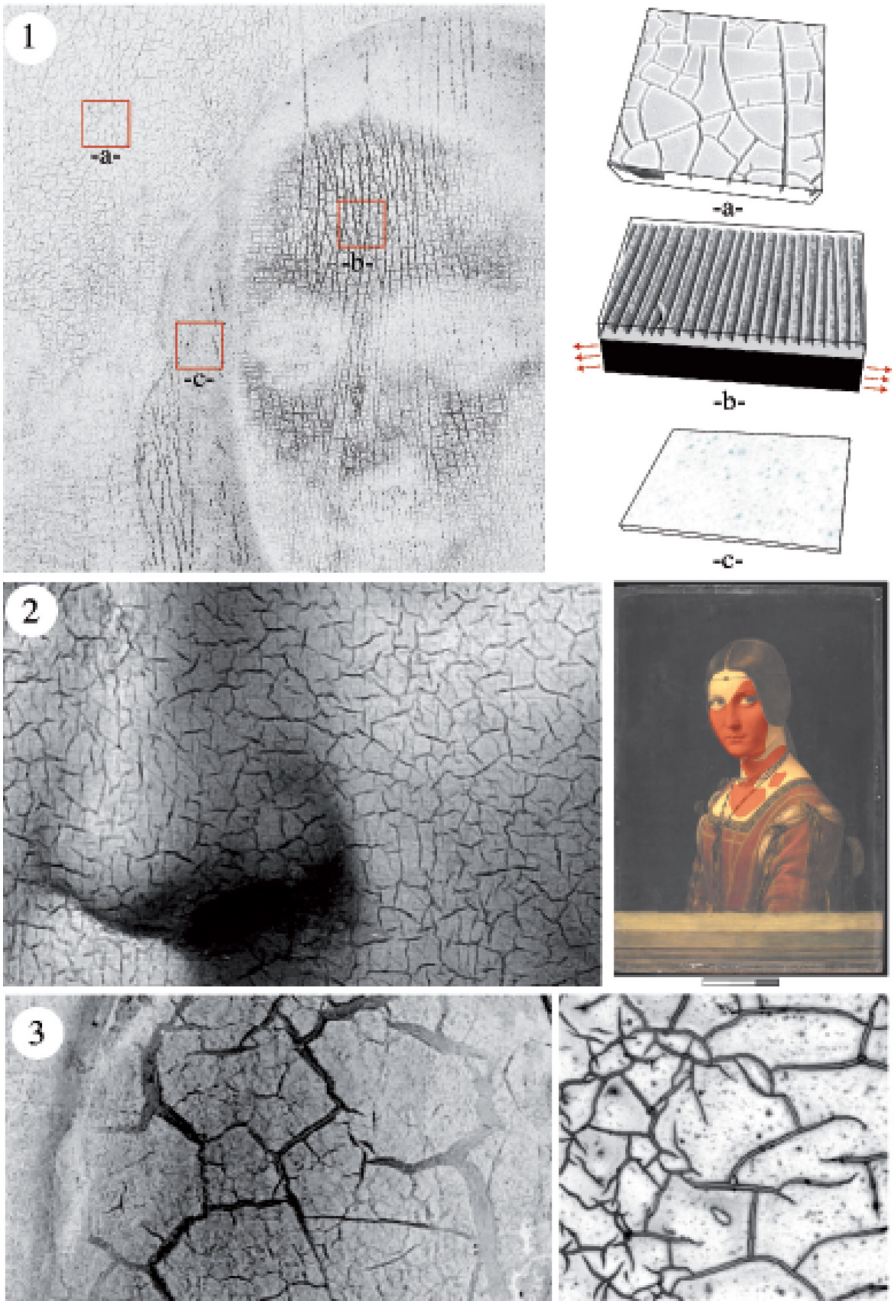

FIG. 1. Various crack patterns in pictorial layers. (1) Crack patterns in some parts of *Mona Lisa* (multispectral imaging of the pictorial layer in: la Joconde, Essai scientifique, collective work under the direction of C. Lahanier, Codex Images International, 2007), and similar patterns in modeled systems; (*a*) hierarchical formation of drying cracks in a drying colloidal layer (100 μ m thick), associated with isotropic aging cracks in the sky of *Mona Lisa*; (*b*) array of parallel cracks in a brittle colloidal layer (20μ m thick) on a stretched sublayer, associated with deep cracks in the carnation of *Mona Lisa*; (*c*) crack-free layer (2 μ m thick), and associated thin layer using the Sfumato techniques in *Mona Lisa*. (2) Junction cracks in a region of the face of *la Belle Ferronnière from Leonardo da Vinci* Copyright C2RMF/L.Pauchard; this pattern is present in region colored in translucent red of the painting. (3) Crack network exhibiting large aperture in a region of *Jeanne d'Arc en prison* of Louis Crignier (Musée de Picardie, Amiens, France, Copyright C2RMF/L. Pauchard) at left and the associated crack pattern in a modeled system at right.

particles approach each other until the formation of a close-packed solid (Figure 2-1).

At the final stage of the drying process, a layer of approximately constant thickness (about 100 μm) covers about 70% of the total surface area. The multi-layered structure is investigated by considering the drying process of a layer on a sublayer. The last is either a glass surface carefully cleaned, exhibiting a stiffness much larger than the layer stiffness, or a solid film of a controlled volume fraction $(1-\phi)$ for stiff and ϕ for soft nanoparticles.

B. Mechanical properties measurements

Measurements of the layer's mechanical properties are performed using indentation testing (MHT-CSM Instruments Micro Indentation Testing)[11,12] with a spherical indenter of radius $R = 0.25$ mm (Figure 3-1).

Measurements are performed on layers of 100 μm thick on a glass slide. We note h, the thickness of the solid layer. Starting with the indenter in contact with the surface of the solid film, the tip is driven inside the sample with a loading speed of 100 mN/min until a maximum load $F_m = 100$ mN. The applied force is then measured as a function of the penetration depth, p. Note that the choice of the value F_m is such that the external pressure exerted by the tip, F_m/S (S being the projected surface of the tip on the film), is close to the capillary pressure $|P_{cap}| \sim 10^8$ Pa exerted by the air/solvent meniscii at the evaporation surface of the layer.

For $\phi < 0.5$, the response of the material is well fitted by the Hertz contact law over the range of indentation depths as shown in the load-displacement curve in Figure 3-2 (the layers are assumed to be purely elastic within the limits of small deformation). Thus, the applied indentation force F before plastic deformation is determined by[13]

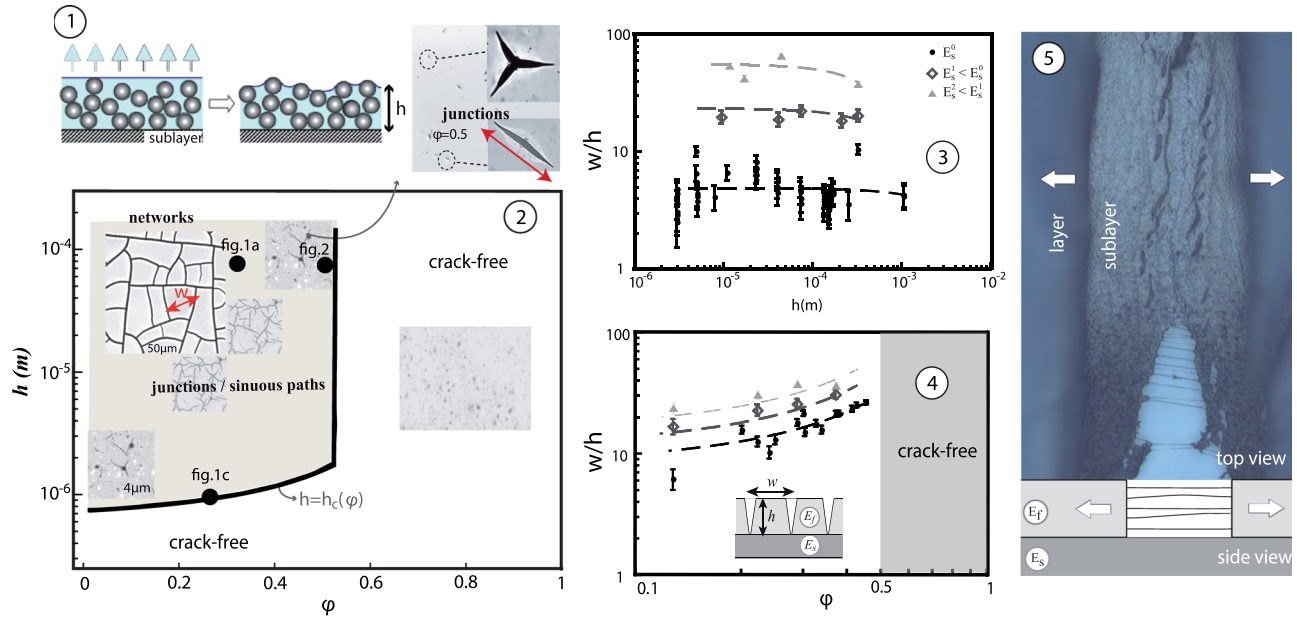

FIG. 2. Crack pattern morphologies diagram in modeled systems. (1) Formation of a solid layer: the drying process of a solid + liquid dispersion. (2) Schematic diagram of classical crack patterns as a function of layer thickness h, and composition ϕ. (3) Variations of the dimensionless crack spacing, w/h, for three various sublayers. (4) Variations of the dimensionless crack spacing, w/h, with the layer composition, ϕ, for three various sublayers. (5) Image in top view and sketch in side view: an opening crack in the layer induces an opening crack in the sublayer as an evidence of the strong adhesion between the layer and sublayer.

$$F = \frac{4\sqrt{R}}{3(1-\nu^2)} E(\phi) p^{3/2}, \tag{1}$$

assuming the spherical indenter of radius R to be perfectly rigid, ν being the Poisson ratio of the layer (we use the value $\nu = 1/3$). The macroscopic elastic response $E(\phi)$ is obtained by the average over the three types of contacts such as[13]

$$\frac{E(\phi)}{(1-\nu)} = 4\phi(1-\phi)\left(\left(\frac{e_H}{(1-\nu_H)}\right)^{-1} + \left(\frac{e_S}{(1-\nu_S)}\right)^{-1}\right)^{-1} + \frac{(1-\phi)^2 e_S}{(1-\nu_S)} + \frac{\phi^2 e_H}{(1-\nu_H)}, \tag{2}$$

where we used the values, $e_H = 10^4$ MPa for the elastic modulus of the stiff particles, $e_S = 30$ MPa for the elastic modulus of the soft particles, and $\nu_H = \nu_S = 0.3$.[14]

Up to $\phi = 0.5$, an increase in the viscous dissipation is revealed (this behaviour was also highlighted by creep measurements). Visco-elastic materials are then conventionally analyzed in terms of mechanical models such as Maxwell model where a viscosity term η quantifies the time-dependent property of the material. Thus, for $\phi > 0.5$, the load-displacement curves satisfy

$$F = \left(\frac{4\sqrt{R}}{3(1-\nu^2)} E(\phi) + \frac{4\sqrt{R}}{3}\eta(\phi)\frac{d}{dt}\right) p^{3/2}, \tag{3}$$

where the layer is now characterized by an elastic term, $E(\phi)$, and a viscous one, $\eta(\phi)$. Moreover, a timescale of the stress release in the material can be defined as $\eta(\phi)/E(\phi)$.

The mechanical properties measured in a given layer strongly depend on the moment the indentation test is done. Even if the measurements were performed after cracks formed, this duration appears to be the single parameter to fit measurements by indentation testing and the theoretical elastic response $E(\phi)$ (Figure 3-3). In the following, the elastic modulus of the film is denoted by $E \equiv E_f$, while the elastic modulus of the substrate is denoted by $E \equiv E_s$.

C. Crack pattern morphology parameters

As the drying proceeds, shrinkage is frustrated by adhesion on a sublayer. This leads to non-uniform shrinkage of the layer causing large tensile stresses as a driving process for crack formation. Under fixed drying conditions, morphologies of cracks depend on (i) the layer thickness, (ii) its composition modeled by a binary mixture of stiff and deformable particles, and (iii) the sublayer mechanical properties. Dependence of these three physical parameters on crack patterns are discussed below, and the results are presented in Figure 2. Patterns of cracks are presented in Figure 2-2, in the parameter space h, the thickness of the layer, and ϕ, the volume fraction of deformable particles.

(i) For a given composition, e.g., ϕ constant, below a critical thickness h_c such as

$$h_c = \Gamma E_f/(Z\sigma^2), \tag{4}$$

films are uniform and free of cracks (here, Γ is the relevant fracture resistant, E_f is the plane strain elastic modulus of the layer, Z is a dimensionless number that depends on the cracking pattern and elastic mismatch of both the layer and the sublayer, and σ is the drying stress).[7,15] Physically, the elastic energy stored in the layer is not sufficient to nucleate cracks (*crack-free region* in the diagram). The quantity h_c is plotted as a function of ϕ in Figure 2-1 using Equation (4)

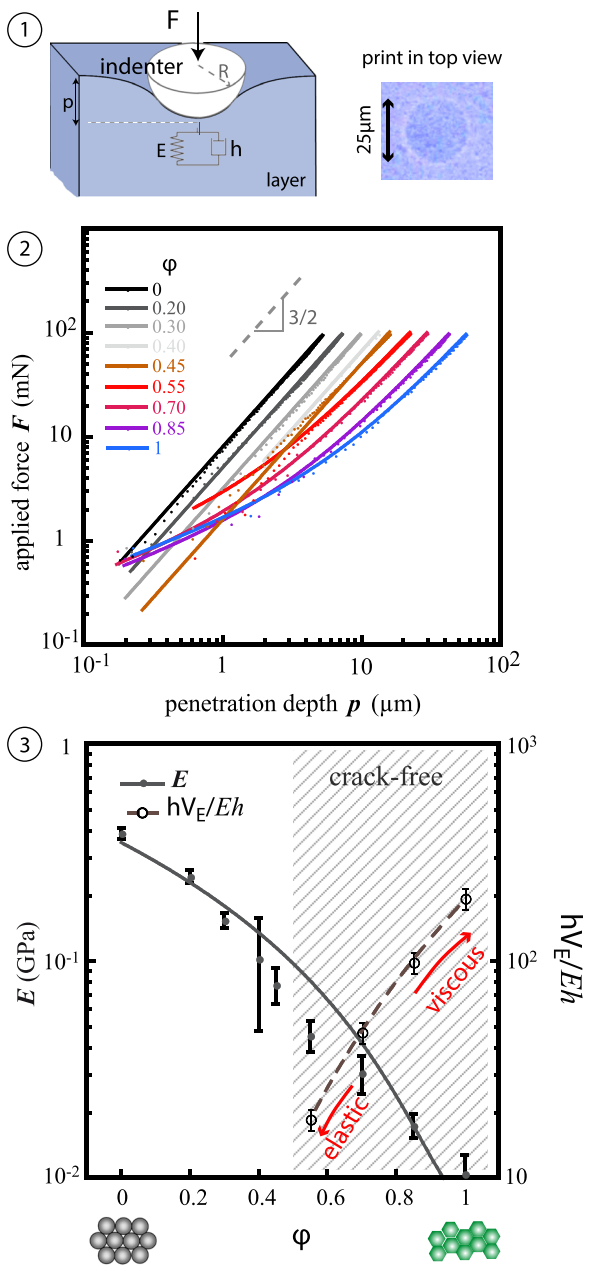

FIG. 3. Mechanical characterization of modeled systems. (1) Schematic representation of the spherical tip-film interaction; optical micrograph of the print at the film surface after the spherical tip has been removed. (2) Indentation load-displacement (F-p) responses for different proportions in deformable particles ϕ in a log-log scale. Measurements of the applied indentation force F as a function of the penetration depth p are well fitted by the Hertz contact theory describing the elastic contact problem. Lines correspond to theoretical predictions. (3) Macroscopic elastic response, E, of solid layers, and ratio of the time rise, $\frac{\eta}{E}$, to the drying time scale, $\frac{h}{V_E}$, as a function of the film compositions in semi-log scale; the dashed line is a guide for the eyes.

assuming the variations in ϕ only through E_f. Up to h_c, a wealth of different patterns can be observed.[8] The crack density is low and depends on the distribution of nucleation sites (defects) in the layer.[10,16] For thicker layers, crack growth stops shortly after their initiation resulting in isolated junctions: linear or star-like junctions, centered around the nucleation sites, predominate (see inset in Figure 2-2). For still thicker films, cracks propagate along sinuous paths that result in a partial connected network. Then, channeling cracks are formed successively resulting in a complete connected network (*networks* region). In the last case, the hierarchical formation of cracks divides the plane into polygonal adjacent fragments.[17]

(ii) Similar crack morphologies can be observed at constant layer thickness but for different layer compositions. The layer composition can be tuned by varying the volume fraction in both the deformable particles, ϕ, and stiff particles, $1-\phi$. For layers with ϕ higher than 0.5, indentation responses demonstrate that the film is viscoelastic. The viscous properties result as an inhibitor of cracks in the layers (crack-free region in the diagram). For ϕ smaller than 0.5, variations in the composition of the film allow one to recover the crack patterns depicted above, such as patterns with isolated junctions, sinuous paths, or complete connected network of cracks. In this last case, a fragment size, w, can be defined as a physical parameter to simply quantify the crack pattern.

(iii) Generally, for given consolidation kinetics and under purely elastic layered structure, the quantity w is a function of the layer thickness and the elastic moduli of both the sublayer, E_s, and the layer, E_f, as $w = f(h, E_f, E_s)$. The measurements for the evolution of w/h, for three different sublayers, respectively, as function of h and ϕ, are reported in Figures 2-2 and 2-3.

Measurements show that the fragment size linearly increases with the layer thickness (Figure 2-3). Moreover, the mismatch between the elastic modulus of the layer and sublayer impacts the fragment size. With a soft sublayer, the layer behaves as if it was not constrained and the fragment size is higher than with glass substrate (see Figure 2-4). When the layer becomes too soft, $\phi > 0.5$, it remains free of cracks (Figure 2-4). Final deformation can be observed in Figure 2-5 in an opening crack on a soft sublayer; as the crack is opening, two edges of a crack are moving apart and one can see distinct shreds of matter between the two edges which attests to no slip with the sublayer and strong adhesion.

D. Model for crack spacing

The dependence of the crack spacing, with the thickness of the layer, or, with the type of sub-layer, is a tricky task, and several authors have proposed some theoretical laws with different degrees of complexity.[10,16,18] Goehring *et al.* propose a review on the different crack pattern morphologies in materials, at different scales.[19] Smith and Sharp[20] have evidenced experimentally that the stress in a drying film is concentrated at the free surface, due to the action of the capillary forces, and decay over a small characteristic length within the film on the order of the particle size. Thus, we consider a slice of region, limited by two nucleation centers, laterally spaced by the quantity w, where we assume that the stress is concentrated. The depth, a, of this region is close to the particle size. The condition for the propagation of an opening crack in the thickness of the layer h is obtained by balancing the stored elastic energy $\frac{1}{2}E_f\epsilon^2 wa$ of the slice with the surface energy required to open a crack in the thickness

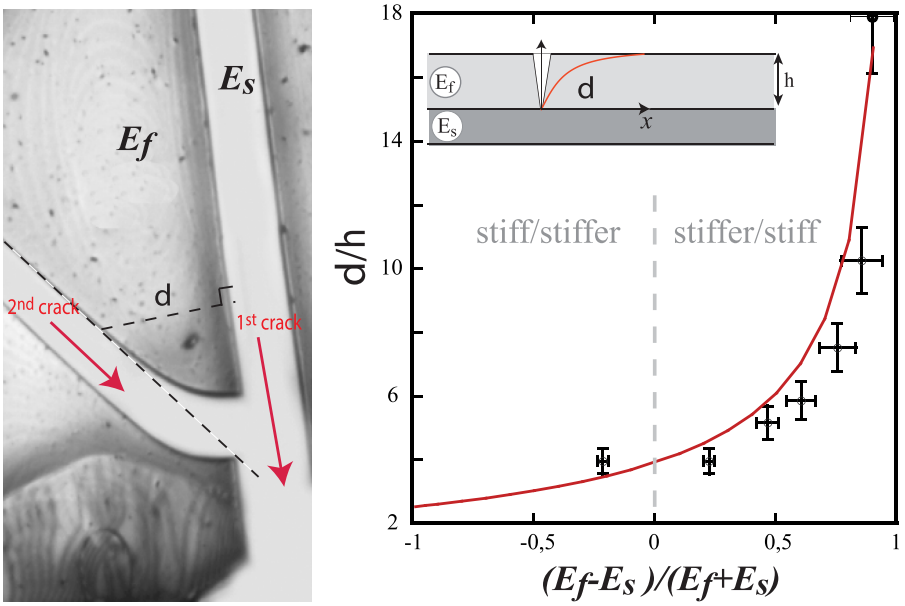

FIG. 4. Connexion between cracks: a way to investigate the multi-layered structure. The interaction is quantified as a function of the elastic modulus mismatch between the layer and the sublayer. Line is theoretical predictions.

layer $2\Gamma h$ when the strain ϵ in the film reaches a maximum value, say, ϵ_m. This maximum deformation between the sublayer and the layer should not exceed 10% (this deformation is estimated through the measurements of the aperture of the cracks). When the sublayer is infinitely stiff, assuming no slippage between the layer and the sublayer, the layer behaves as it was not constrained and the crack spacing can be expressed as

$$w/h \sim 4\Gamma/(E_f a{\epsilon_m}^2). \tag{5}$$

On the contrary, on a less stiff substrate, the sublayer induces some stress in the layer, and an additional strain ϵ_s in the sublayer has to be considered.

The strain ϵ_m in the layer can be expressed as $\epsilon_m \sim \epsilon_s + \epsilon$ with ϵ_s negative so that the strain in the film is reduced compared to the case of a stiff sublayer. Another expression based on the balance of forces at the interface relates the strain in the film and in the substrate: $\epsilon_s \sim E_f/E_s\epsilon$. The dimensionless crack spacing is now

$$w/h \sim 4\Gamma/(E_f a\epsilon^2)(1 + E_f/E_s)^2. \tag{6}$$

Values for E_f and E_s are deduced from indentation testing. Measurements on modeled systems presented in Figure 2-3 are well fitted by this scaling law.

E. Connections between cracks

As mentioned above, the morphology of a crack pattern and, in particular, the crack spacing, depends strongly on the way the sublayer resists the deformation and the key parameter is the ratio between the elastic moduli of the layer and the sublayer, E_f/E_s. Another typical length-scale is the length-scale over which the stress relaxes in the vicinity of a crack. This value depends, like the crack spacing, on the elastic properties of the layer and the sublayer. Indeed, the crack pattern forms through propagation of successive generations of cracks, and the first generation defines then the boundary conditions for the mechanical stress field that will govern the formation of future cracks. Therefore, at some distance from a pre-existing crack path, the stress remains unrelaxed on a length-scale, δ, due to the constraint of the substrate. A second crack will change its direction of propagation when its approaches the first one at a distance less than δ (see Figure 4). The length-scale, δ, over which stresses relax can be easily measured on a crack pattern as the distance from which the latter crack curve intersects the earlier one.

This length-scale depends on the way the substrate or the sublayer resists the deformation as the crack propagation. Thus, the height-average film stress normal and parallel to a crack face increases exponentially from the crack position to recover the stress field of the film at the distance δ from the crack. δ is found for small deformations, to be equal[21] to $\delta/h = \frac{\pi}{2} g(\alpha, \beta)$, where g is a numerical function which depends on the Dundurs parameters α $(-1 < \alpha < 1)$ and β $(0 < \beta < \alpha/4)$ which depend on the plane-strain elastic moduli and on the Poisson ratio of both the film and the sublayer (β typically has only little influence on the results compared to the influence of α). In the limit of a very soft sublayer, δ diverges and the film behaves as if it is not constrained. Depending on the elastic mismatch between the film and the sublayer, δ can vary from $2.h$ (for layers with the same elastic moduli) to $1.2.h$ where the sublayer is very brittle. To test this behavior experimentally, we consider a system of two layers made of the binary mixture of stiff and deformable particles used before and tune the elastic properties of each layer by changing the proportion of soft and stiff particles. The elastic moduli of each layer can be estimated by indentation testings separately. For each experiment, we report the measured values of δ/h as a function of the elastic mismatch between the layer and the sublayer, e.g., α. The theoretical predictions related to the Dundur model fit the experimental data perfectly well. This method could then be applied for paintings to deduce mechanical properties of sublayers using only optical measurements on the crack pattern. This result indicates the interest of using model systems for testing methods and scaling laws for determination of mechanical properties of a system, without any intrusive action which ensure no damage on

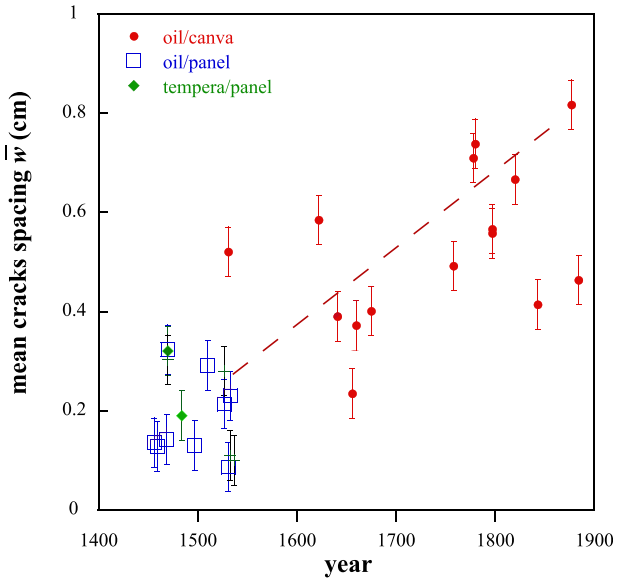

FIG. 5. Comparison of the mean crack spacing, $\bar{w}$, over years in real pictorial layers. Measurements have been carried out on isotropic crack patterns, specifically in carnations, on high spatial resolution images provided by Cultural Institute of Google, The Art Project. Dotted line is a guide for the eyes.

the painting. This requires to collect measurements on crack patterns on real paintings. This could be achieved, thanks to very high resolution images of the paintings.

F. Measurements on real paintings

We have proceeded to measurements of w, on paintings from the beginning of the fifteenth century to the beginning of the nineteenth century. The paintings selected were made of various supports, canvas or panel, and with various kinds of binding media such as oil or tempera. Only the isotropic crack patterns, which reveal aging cracks, in the carnations have been considered (face of portrait). The results are reported in Figure 5.

Each point corresponds to the mean crack spacing deduced for a single painting. Over years, the degree of stiffening of a pictorial layer is irretrievably modified. Indeed, the paint layer gets stiffer and stronger,[1,5] increasing the resistance to crack formation. Apart from the fact that the mean crack spacing increases over centuries, thanks to the evolution of the material and mainly due to the addition of various components into the paint, measurements highlight the influence of the support or of the binding. In particular, the number of cracks appears to be larger in a tempera paint layer on a wood panel than with oil binding paint layer on a canvas panel. Despite the large variety of materials, supports, or environmental parameters, all the data through five centuries present a relatively small dispersion. It could then be possible by tuning the composition of a model system (mixture of stiff and deformable particles) to reproduce behaviors of old (few centuries) or recent paintings (few tens years).

IV. CONCLUSION

We propose in this paper to reproduce the crack patterns observed in paintings by using model systems made of a mixture of stiff and deformable colloidal particles. The use of these model systems, well controlled and characterized, aims to test some theoretical predictions and to deduce qualitative and quantitative values of the mechanical properties of the material. Two main physical parameters are considered to recover the large majority of crack patterns observed in paintings:

(i) The ratio between stiff and soft particles; it is then possible to tune and control the mechanical properties of the model systems.
(ii) The initial volume of liquid to change the thickness h of the dried final porous film.

The mechanical characterization of model systems is achieved, thanks to micro-indentation measurements which provide the elastic modulus and the time for stress relaxation for visco-elastic systems. A kind of phase diagram in the parameter space h and ϕ (the proportion in deformable particles) is then deduced. By changing h or ϕ, we recover some crack patterns observed in paintings. The evolution of the mean size fragment of a crack pattern with the thickness of the layer is well fitted by a scaling law which takes into account the role of the substrate. We then test the Dundur theory relative to the typical length-scale for the stress relaxation in a layer constrained by a sub-layer. By changing the ratio between stiff and soft particles in the suspension, one can tune the mismatch between the layer and the sub-layer. Measurements of the length-scale for the stress relaxation performed on the crack patterns are well fitted by the Dundur model. By applying this theory to paintings, it becomes possible to deduce elastic properties of the sub-layer simply by measuring the length-scale of the stress relaxation on crack patterns. We propose here a completely noninvasive method which consists in measuring length-scales to deduce some mechanical properties of the system. These experiments show that crack morphologies appear to be specifically related to the material and the way the cracks are generated. In addition, we show that cracks induced by desiccation in colloidal systems exhibit generic morphologies. These results support the idea that crack patterns can provide much information on the matter of paintings and that model systems can be used for that specific purpose.

ACKNOWLEDGMENTS

The authors want to thank M. Menu and C. Thill for fruitful discussions and N. Ribe for a careful reading of the manuscript. We acknowledge financial support through the Funding agency: Investissement d'Avenir LabEx PALM (Grant No.: ANR-10-LABX-0039). We thank A. Aubertin, L. Auffray, and R. Pidoux (FAST-University Paris Sud) for engineering and technical support.

[1]M. F. Mecklenburg and C. S. Tumosa, "Mechanical behavior of paintings subjected to changes in temperature and relative humidity," in *Art in Transit*, edited by M. F. Mecklenburg (National Gallery of Art, Washington, D.C., 1991) pp. 172–214.
[2]L. Pauchard, V. Lazarus, B. Abou, K. Sekimoto, G. Aitken, and C. Lahanier, Reflets Phys., Soc. Fr. Phys. **3**, 5–9 (2007).
[3]S. Bucklow, "The description of craquelure patterns," Stud. Conserv. **42**, 129–140 (1997).

[4]G. L. Stout, "A trial index of laminal disruption," J. Am. Inst. Conserv. **17**, 17–26 (1977).
[5]M. F. Mecklenburg, "Some aspects of the mechanical behavior of fabric supported paintings," Smithsonian Institution, Washington, DC, Report No. 12–15, 1982.
[6]P. de Willigen, *A Mathematical Study on Craquelure and Other Mechanical Damage in Paintings*, WBBM Report Series 42/MOLART Report Series 2 (Delft University Press, 1999).
[7]A. Atkinson and R. M. Guppy, J. Mater. Sci. **26**, 3869 (1991).
[8]V. Lazarus and L. Pauchard, Soft Matter **7**, 2552 (2011).
[9]J. H. Prosser, T. Brugarolas, S. Lee, A. J. Nolte, and D. Lee, Nano Lett. **12**(10), 5287–5291 (2012).
[10]A. Groisman and E. Kaplan, Europhys. Lett. **25**, 415 (1994).
[11]J. Malzbender, J. M. J. den Toonder, A. R. Balkenende, and G. de With, "Measuring mechanical properties of coatings: A methodology applied to nano-particle-filled sol-gel coatings on glass," Mater. Sci. Eng., R **36**, 47–103 (2002).
[12]K. Vanstreels, C. Wu, M. Gonzalez, D. Schneider, D. Gidley, P. Verdonck, and M. R. Baklanov, Langmuir **29**(38), 12025–12035 (2013).
[13]K. L. Johnson, *Contact Mechanics* (Cambridge University Press, 1985).
[14]L. Pauchard, B. Abou, and K. Sekimoto, Langmuir **25**, 6672 (2009).
[15]J. W. Hutchinson and Z. Suo, in *Mixed Mode Cracking in Layered Materials*, edited by J. Hutchinson and T. Wu (Academic Press, 1992), Vol. 29, pp. 63–191.
[16]H. Colina and S. Roux, Eur. Phys. J. E **1**, 189 (2000).
[17]S. Bohn, L. Pauchard, and Y. Couder, Phys. Rev. E **71**, 046214 (2005).
[18]T. X. Bai, D. D. Pollard, and H. J. Gao, Nature **403**(6771), 753–756 (2000).
[19]L. Goehring, A. Nakahara, T. Dutta, S. Kitsunezaki, and S. Tarafdar, *Desiccation Cracks and their Pattern* (Wiley, 2015).
[20]M. I. Smith and J. S. Sharp, Langmuir **27**(13), 8009–8017 (2011).
[21]J. L. Beuth, Int. J. Solids Struct. **29**, 1657–1675 (1992).